Materials Chemistry and Physics xxx (2016) 1–10

Contents lists available at ScienceDirect

Materials Chemistry and Physics

journal homepage: www.elsevier.com/locate/matchemphys

Structural and electrical properties of SnS_2 thin films

A. Voznyi [a, b, *], V. Kosyak [a, b], A. Opanasyuk [a], N. Tirkusova [a], L. Grase [b], A. Medvids [b], G. Mezinskis [b]

[a] Sumy State University, 2, Rymsky Korsakov Str., 40007 Sumy, Ukraine
[b] Riga Technical University, 3/7, Paula Valdena Str., LV-1048 Riga, Latvia

HIGHLIGHTS

- Deposition of SnS_2 thin films by the close-spaced vacuum sublimation method.
- The layers have single-phase hexagonal structure of 2H–SnS_2 polytype.
- The conductivity of the SnS_2 films depends on growth conditions and changes in the range from 1.8×10^{-4} to 10^{-7} $(Om \cdot cm)^{-1}$.
- Activation energies of 0.25 and 0.26 eV in SnS_2 films were found from temperature conductivity measurements.

GRAPHICAL ABSTRACT

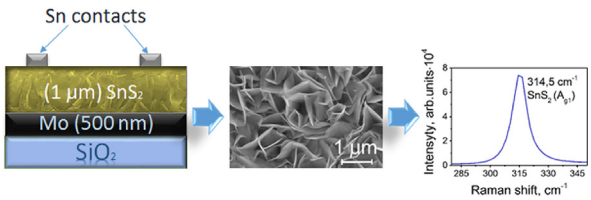

ARTICLE INFO

Article history:
Received 29 September 2015
Received in revised form
22 December 2015
Accepted 13 January 2016
Available online xxx

Keywords:
Thin films
Chalcogenides
Electron microscopy
Semiconductors
Raman spectroscopy and scattering
Electrical properties

ABSTRACT

The effect of substrate temperature on the structural and electrical properties, phase composition, and surface morphology of tin disulfide thin (SnS_2) films obtained by the close-spaced vacuum sublimation (CSS) method was studied.

Scanning electrical microscope (SEM) images of the samples showed that all of the films were polycrystalline with an average grain size of 0.7–1.2 μm. The average thickness of the thin films was 1 μm.

Energy dispersive spectroscopy (EDS) analysis showed that all layers had close to stoichiometric atomic composition. Namely, the concentrations of tin and sulfur were 35 and 65% respectively.

X-ray diffraction (XRD) study indicated that the samples obtained at 473–723 K mostly contained hexagonal phase SnS_2 with high texture along the (002) crystallographic plane. The values of the lattice constants (a and c) of SnS_2 thin films increase monotonically with substrate temperature from 0.3637 to 0.3647 nm and from 0.5703 to 0.5743 nm, respectively.

Investigation of the SnS_2 films by Raman spectroscopy confirmed the results of XRD studies, namely that the layers have single-phase hexagonal structure of 2H polytype.

Studies of the electrical properties of SnS_2 thin films showed that the conductivity of the films changed from 1.8×10^{-4} to 10^{-7} $(Om \cdot cm)^{-1}$. Analysis of the I–V characteristics in the space-charge limited current (SCLC) mode made it possible to define ($E_{t1} = (0.52–0.55)$, $E_{t2} = (0.46–0.49)$, $E_{t3} = (0.43–0.45)$, and $E_{t4} = (0.35–0.39)$ eV), the localized states energy depths in the band gap of the SnS_2 thin films. The concentration of these localized states exceeds 1.31×10^{14} cm^{-3}. Also, from the measurements of temperature dependent conductivity, several localized states with activation energies of 0.25 and 0.26 eV states were determined.

* Corresponding author. Sumy State University, 2, Rymsky Korsakov Str., 40007 Sumy, Ukraine.
E-mail address: andrey.vozny@gmail.com (A. Voznyi).

http://dx.doi.org/10.1016/j.matchemphys.2016.01.036
0254-0584/

1. Introduction

Recently, the interest of researchers in materials with a 2D crystal structure, such as MoS_2, WS_2, SnS_2, and so on, has increased significantly [1–3]. Unique electrical properties of these compounds are associated with the layered structure and specific properties of the surface; namely, crystals of transition metal dichalcogenides consist of stacked layers that interact via weak van der Waals forces, while intralayer bonding is primarily due to the strong covalent bonding between the atoms. This allows the formation of stable thin crystals with thickness down to a few atomic layers. These properties make such materials promising for the creation of devices for energy storage, light emission, electron emission, catalysis, and sensors [4–8].

SnS_2 has a CdI_2-like crystal structure that consists of densely packed atomic layers of tin placed between two layers of sulfur. This compound can exist in the form of several polytypes [9,10]. The band gap of SnS_2 changes in the range of 2.12–2.44 eV depending on the method of obtaining material and their polytype [7,8,11–13]. SnS_2 has n-type conductivity, a high optical absorption coefficient > 10^4 cm^{-1} [14,15], and relatively high charge carrier mobility of 18.3–230 $cm^2/V\cdot s$ [7,8,16,17]. These properties make it promising for use in thin film solar cells. In particular, SnS_2 is considered to be an alternative material to a conventional CdS window layer [8,13]. The advantages of SnS_2 are that it is non-toxic and its constituent elements (Sn and S) are cheap and Earth-abundant.

Tin disulfide thin films can be obtained using the following methods: ionic layer adsorption and reaction (SILAR) [18], spray pyrolysis [14,19–21], thermal vacuum evaporation [13,22], plasma-enhanced chemical vapour deposition (PECVD) [15], and dip coating [23]. Each of the methods of obtaining SnS_2 thin films has its advantages and disadvantages. For example, the spray pyrolysis method allows one to obtain a low-cost thin layer of semiconductor. However, thin film obtained by this method has low crystal quality, which could be improved by post-growth annealing of material in toxic H_2S gas [23,24]. The CSS method for deposition of SnS_2 thin films was used only in [25]. This method is also widely used for obtaining high quality thin films of binary semiconductors [26–28]. However, the possibility of deposition of single-phase SnS_2 films by the CSS method without the application of post-growth treatment has not been studied carefully.

SnS_2 films often include secondary phases of Sn_2S_3 or SnS, which may significantly affect the structural, optical, and electrical properties of the material [29,30]. One of the most effective methods of phase analysis of Sn_xS_y compounds is Raman spectroscopy [31,32]. This method is mostly used together with XRD and allows one not only to study phase composition but also to identify polytypes in the samples [29,33].

The structural, optical, and electrical properties of SnS_2 bulk crystals have been studied quite well [6–8,34–38]. On the other hand, the physical properties of the SnS_2 films and their dependence on the growth conditions are still insufficiently studied.

In order to create SnS_2-based high-performance devices, it is necessary to control electrically active defects in the material. But the currently available results on the electrical properties of SnS_2 crystals and films do not provide an overall picture regarding the parameters and nature of charged donor (acceptor) defects and trap centres. In particular, in works [39–41] only values of activation energies are given without any detailed discussion of their origin. This could be explained by the fact that, in contrast to SnS [42,43], the theoretical calculation of the formation and ionization energies has still not been performed.

This paper presents the results of a comprehensive study of the influence of substrate temperature on the structural and electrical properties and phase composition of SnS_2 thin films obtained by the CSS method. Also, the parameters of localized states (LSs) in the band-gap of SnS_2 thin films were determined from analysis of the current–voltage characteristic and temperature-dependent conductivity measurements.

2. Experimental

SnS_2 thin films were obtained in a VUP-5M vacuum chamber by the CSS method. The pressure of residual gases in the chamber was no more than 5×10^{-3} Pa. A detailed description and scheme of the device for obtaining the thin films are available in [28].

Samples were deposited on ultrasonically cleaned Mo (500 nm thick) coated glass substrates. The stoichiometric powder of SnS_2 was used as an initial material for evaporation. The temperature of the evaporator was T_e = 948 K. The substrate temperature (T_s) varied in the range of 473–723 K. The duration of deposition was 4 min.

The surface morphology and chemical composition of the thin films was investigated using an FEI Nova NanoSEM 650 Schottky field emission scanning electron microscope (SEM) with an integrated Apollo X energy dispersive spectroscope (EDS) for the chemical composition analysis using standardless energy techniques. The following parameters were used in the EDS experiment: an accelerating voltage of 15 kV, a detector resolution of 125.4 eV, a working distance of 7 mm, and a spot size of 5.5. The calculation of the concentrations was determined by averaging of results for at least 10 measurements from different points on the surface. The thickness was measured by SEM directly from the cross-section of the samples.

In order to study the microstructure of the surface and to estimate its roughness, an NT-MDT atomic force microscope (AFM) was used.

The study of the structural properties and phase composition of the tin disulfide thin film was carried out with the help of a DRON-4-07 diffractometer using CuK_α radiation and Bragg-Brentano configuration. The range of the 2θ angle varied from 10° to 80°. Identification of the crystal phases was performed with the Crystallography Open Database (COD).

The average size of the coherent scattering domain (CSD) was determined by physical broadening of the diffraction lines using the Scherrer equation [44].

$$L = \frac{k\lambda}{\beta \cos\theta} \quad (1)$$

where k is a coefficient that depends on the grain size (k = 0.9), and β is the physical broadening of corresponding X-ray lines.

The texture quality of the SnS_2 thin films was estimated by the Harris method [44]. The pole density was calculated by using the expression given in [26].

$$P_i = \frac{(I_i/I_{0i})}{\frac{1}{N}\sum_{i=1}^{N}(I_i/I_{0i})} \quad (2)$$

where I_i and I_{0i} are the total intensities of diffraction peaks from the film and reference, respectively, and N is the number of lines present in the X-ray diffraction pattern.

After that, the dependencies of P_i on (hkl) and P_i on φ were plotted, where φ is the angle between the axis of the texture and the direction perpendicular to the corresponding (hkl) crystallographic plane. The orientation factor was calculated using the equation presented in [26].

Please cite this article in press as: A. Voznyi, et al., Structural and electrical properties of SnS_2 thin films, Materials Chemistry and Physics (2016), http://dx.doi.org/10.1016/j.matchemphys.2016.01.036

$$f = \sqrt{\frac{1}{N}\sum_{i=1}^{N}(P_i - 1)^2} \quad (3)$$

The Nelson–Riley method was used for calculation of the (a, c) lattice constants of the SnS_2 films [44]. This method allows one to obtain the lattice constant of the material to an accuracy of 0.001%.

Raman spectra were measured by using Renishaw's InVia 90V727 Raman spectrometer at room temperature. An Ar ion laser with a wavelength of 514 nm was used as the excitation source. The diameter of the laser spot was 0.7 μm, the power density of the laser beam was 6.78 W/cm^2, and the accumulation time was 20 s.

Measurements of the electrical properties of SnS_2 thin films were performed using Sn/SnS_2/Mo sandwich structures. The electron affinity χ_{SnS2} of SnS_2 is 4.2 eV [45]. Such a high value complicates the selection of a suitable metal for the formation of ohmic contact with n-SnS_2, because in order to obtain ohmic contact with SnS_2, the work function of the contact material should be less than χ_{SnS2}. It is well known that the effect of the metal–semiconductor barrier on I–V measurements could be effectively avoided by doping of the semiconductor, because in this case, the width of the depletion region drops and the charge carriers can tunnel through the depletion region [46]. For this purpose, in order to provide diffusion of Sn into the sample and hence doping of SnS_2 at the surface, the Sn contacts were deposited on as-grown samples using the thermal vacuum evaporation technique at a substrate temperature of 353 K. Taking into account the diffusion of metal atoms into SnS_2 as a result of contact, the application of Sn is more favourable, because, in contrast to any other metals, Sn forms only native point defects in SnS_2 and hence allows the presence of foreign impurities to be avoided.

Mo-coated glass is a commercially available metal-coated substrate that is widely used as a back contact for CdTe, CuInGaSe, and $CuZnSnS(Se)_2$ solar cells [47,48]. The high melting temperature of 2896 K makes Mo ideal for temperature-conductivity measurements at high temperatures because, in this case, the low rate of interdiffusion between metal coating and substrate could be expected. The main aim of making electrical measurements of the films was to study the trap centres by the injection spectroscopy method. This method requires measurements made under a relatively high voltage. Therefore the substrate material should provide good adhesion with the sample. We used Mo as a back contact for CdTe, ZnTe, and ZnS polycrystalline thin films in our previous studies [49,50]. Mo substrates demonstrate good adhesion with thin films of these materials. This allows us to obtain reliable results of injection spectroscopy and temperature-conductivity measurements. The work of function of Mo is 4.53 eV, which may lead to the formation of a Schottky barrier with SnS_2. However, this barrier could be reduced due to the presence of defect states, which is typical for highly disordered polycrystalline material. Also the effect of the Schottky barrier on the transport of free carriers under a high bias voltage could be insufficient due to tunnelling [46].

I–V curves were measured under a direct bias voltage varied with a step of 0.05 V. The current passing through the sample was evaluated by a Tektronix DMM 4020 multimeter. The temperature-dependent conductivity was studied in the temperature range of 298–423 K.

The charge transport mechanism was defined by the differential method developed in [51–54]. It allowed us to establish that the current flow mechanism corresponds to the space-charge limited current (SCLC) mode. Furthermore, the injection spectroscopy (IS) method was used for processing of I–V characteristics. The main equations of the IS method are presented in [52,55] and given below:

$$n_f = \frac{\eta}{2\eta - 1}\frac{jL}{e\mu V} \quad (4)$$

$$n_s = \frac{\rho_0}{e} = \frac{2\eta - 1}{\eta}\frac{\eta - 1}{\eta}\left[1 - \frac{\eta'}{\eta(2\eta - 1)(\eta - 1)}\right]\frac{\varepsilon\varepsilon_0}{eL^2} \quad (5)$$

where j is the density current passing through the sample, and V is the voltage applied to the sample; $\eta = \frac{d(\ln j)}{d(\ln V)}$, $\eta' = \frac{d^2(\ln j)}{d(\ln V)^2}$, $\eta'' = \frac{d^3(\ln j)}{d(\ln V)^3}$, where e is the electron charge, μ is the drift carrier mobility, L is the thickness of the sample, ε0 is the dielectric constant, ε is the permittivity of the material, n_s is the concentration of the trapped carriers in the thin

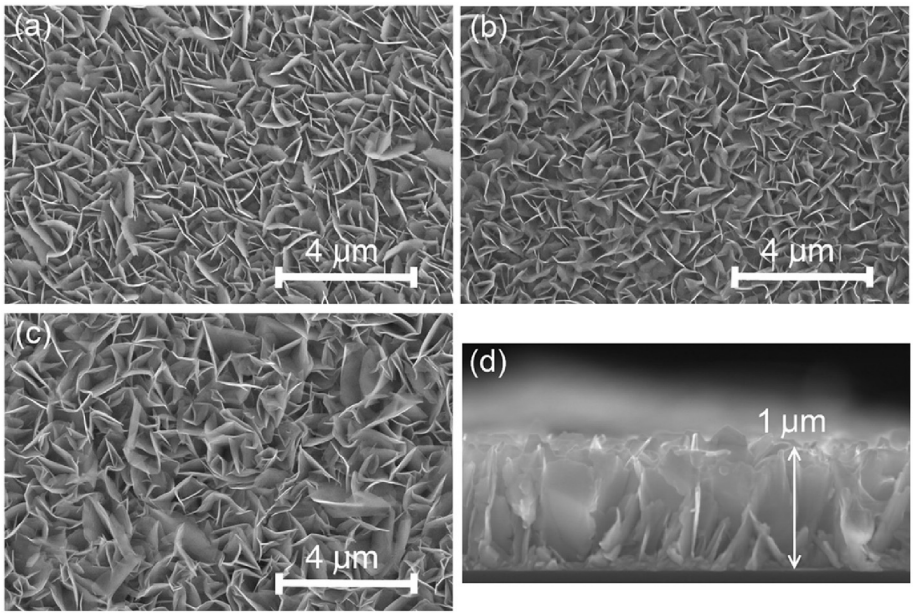

Fig. 1. SEM images of the surface of as-deposited SnS_2 films at 573 K (a), 673 K (b), and 723 K (c) and typical cross-section (d).

Please cite this article in press as: A. Voznyi, et al., Structural and electrical properties of SnS_2 thin films, Materials Chemistry and Physics (2016), http://dx.doi.org/10.1016/j.matchemphys.2016.01.036

film, ρ is the space charge density in the material that limits through the sample current, and n_f is the concentration of free carriers injected into the films.

Using the well-known relation between the concentration of free carriers and the Fermi level energy $n_f = \exp((E_F - E_c)/kT)$ and setting $E_c = 0$, it is easy to determine the energy scale of the LS from Eq. (4):

$$E_F = kT \ln\frac{N_{c(v)}e\mu}{L} + kT \ln\frac{j}{V} + kT \ln\frac{\eta}{2\eta - 1} \quad (6)$$

where E_F is the position of the quasi-Fermi level for injection, k is the Boltzmann constant, T is the temperature, and $N_{c(\upsilon)}$ is the free effective density of states in the conduction (valence) band.

The distribution function of carriers localized at deep centres could be obtained by differentiation of Eq. (5) for the energy:

$$R(E) = \frac{dn_s}{dE_F} = \frac{1}{kT}\frac{2\eta - 1}{\eta}\left[1 + \frac{3(\eta - 1)\eta\eta' - \eta\eta'' + 3\eta'''}{\eta^2[(2\eta - 1)(\eta - 1) - \eta'/2]}\right]\frac{\varepsilon\varepsilon_0}{eL^2}V \quad (7)$$

The distribution function of LS density for the energy $h(E) = dN_t/dE$ as a low-temperature approximation is thought to coincide with the distribution function of localized carriers. However, this leads to some errors in the reproduction of trap distributions as well as in the determination their depth energy (E_t) and concentration (N_t) [52,55].

The joint solution of Eqs. (6) and (7) allows us to find the h(E) distribution function in the band gap of material directly from the experimental SCLC I–V curves. For this purpose it is necessary to define three derivatives at each point of the I–V curve on a log–log scale. Mathematically, this task is reduced to an approximation of the experimental data by a cubic smoothing spline and its differentiation.

In order to determine the parameters of LSs in SnS_2 thin films, the low-temperature approximation of the IS method was used. At the same time, the correction of errors that arise during processing of I–V curves was carried out with the help of simplified expressions proposed by Nespurek and Manfredotti [54,56]. For the calculation of the energy levels of traps in the band gap and their concentration, the method proposed in [52,55] was used. For the calculation, the dielectric constant of the SnS_2 thin films was assumed to be 6.19 F/m, the charge carrier mobility 51.5 $cm^2/V\cdot s$, and the effective density of states in the conduction band 7.32×10^{24} m^{-3} [57]. The spin degeneracy factor of all traps was considered to be equal to 1.

3. Results and discussion

Fig. 1 shows the SEM images of the samples. It was established that the films obtained in the range of the substrate temperature of 473–723 K are polycrystalline and consist of platelet-shaped grains. The average grain size varies in the range of 0.7–1.2 μm and depends on T_s. The thickness of the grains is approximately 100 nm. Similar shape of crystallites in the SnS_2 thin films were also observed in [58–60].

The thickness of the layers was determined by SEM directly from the cross-section. The typical cross-section of tin disulfide thin films is shown in Fig. 1(d). It was determined that the average thickness of the SnS_2 thin films was 1 μm.

The influence of the substrate temperature on the chemical composition of the films was studied by EDS.

It was established that the composition of all investigated films was close to stoichiometric (35 ± 5 and 65 ± 5 at% for Sn and S, respectively). These results are in good correlation with the data given in [14,19,23] for films obtained by spray pyrolysis and dip coating. However, our thin films are more stoichiometric than SnS_2 layers deposited by thermal vacuum evaporation in [13]. It should be noted that scanning of the film surface by EDS reveals their uniform chemical composition. Also, no impurities or inclusions were detected.

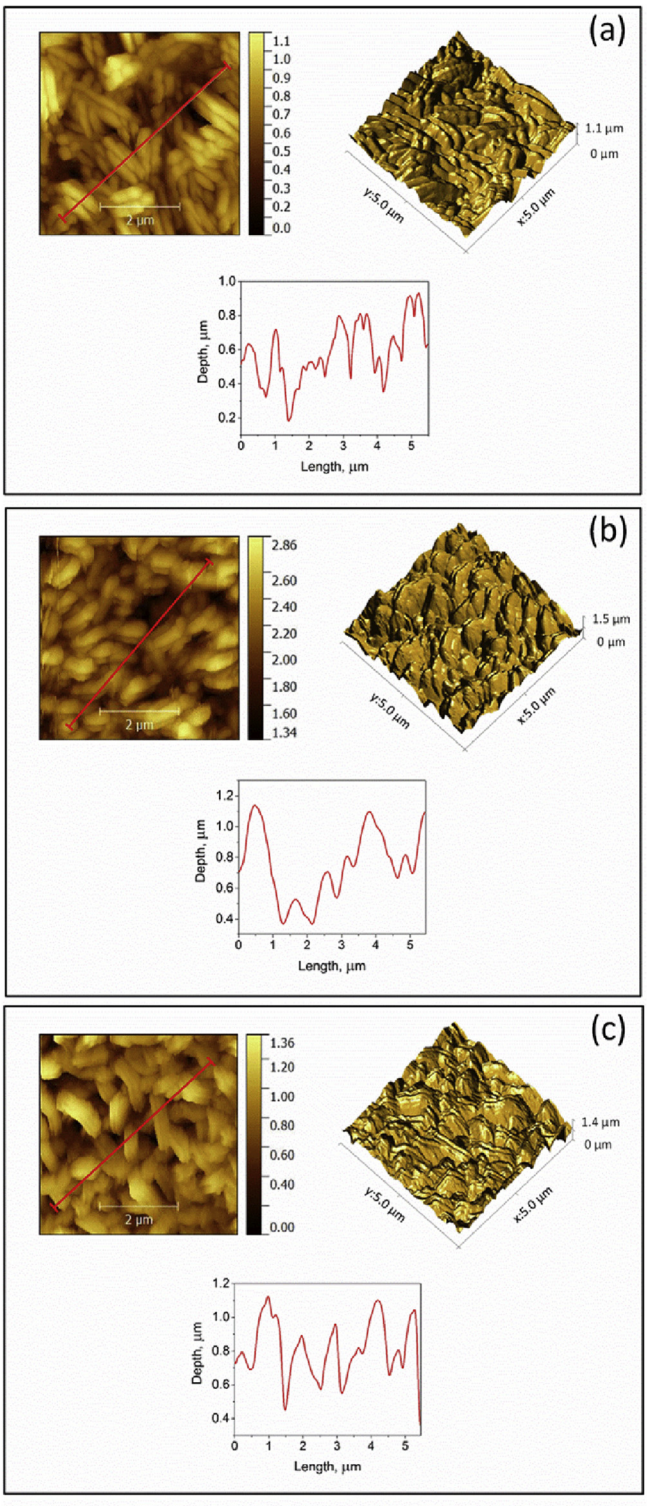

Fig. 2. AFM images of the surface and profiles of as-deposited SnS_2 films at 573 K (a), 673 K (b), and 723 K (c).

The results of AFM study are presented in Fig. 2. As follows from Fig. 2, the thickness of the platelet-shaped grains decreases from bottom to top in the direction perpendicular to the surface (i.e. perpendicular to the growth front). Thus the AFM scan makes it possible to determine that the platelet-like grains' crystallites have a cone-shaped structure. The length of grains of about 0.7 μm for the sample obtained at 673 K (Fig. 2(b)) was slightly less than the length of grains of about 1.5 μm for the samples obtained at 573 K (Fig. 2(a)) and 723 K (Fig. 2(c)). The thickness of grains increased slightly with substrate temperature from 0.2 μm for the sample obtained at 573 K (Fig. 2(a)) to 0.5 μm for the sample obtained at 723 K (Fig. 2(c)). The AFM profiles show high roughness of the samples of about 0.4 μm.

The XRD patterns of the powder and SnS_2 films deposited at different substrate temperatures are shown in Fig. 3. It was found that the detected peaks corresponded to reflections from the (001), (100), (002), (011), (003), (110), (111), and (004) crystallographic planes of hexagonal phases of the SnS_2, the (103), (202), (011), and (305) crystallographic planes of the orthorhombic phase of Sn_2S_3, and the (101) and (211) crystallographic planes of the cubic phases of molybdenum (Mo). The positions of these peaks are in good correlation with the COD database for SnS_2, Sn_2S_3, and Mo (card nos. 96-900-0614, 96-901-1237, and 96-900-8544, respectively). Reflections from the crystallographic planes (001), (100), and (002) of the hexagonal phase of SnS_2 had the strongest intensity, while the intensity of Sn_2S_3-related peaks was very weak. Thus, we conclude that films obtained in the temperature range of 473–723 K contain mostly hexagonal phase SnS_2 with a small amount (<3–5%) of Sn_2S_3 phase.

Calculations by the inverse pole figures method reveals the [002] growth texture in the SnS_2 films. The direction of growth texture coincides with the growth direction of most crystallites. Such growth texture is typical for SnS_2 thin films [19,31,61]. The results of calculation of the orientation factor are shown in Table 1. As follows from Table 1, the growth texture of the layers is very high. For the samples deposited at $T_s = 573$ K, the orientation factor is $f = 4.4$, while an increase in the substrate temperature to $T_s = 673$ K leads to a decrease of the orientation factor to 1.0. With further increases of T_s to 723 K, the growth texture of the layers increases slightly to $f = 1.9$. We previously observed a similar effect of substrate temperature on growth texture in the case of II–VI films obtained by CSS [26].

Table 1
Results of the calculation of the orientation factor (f), lattice constants (a, c), and coherent scattering domain (CSD) size.

T_s, K	Orientation factor, F, arb.unit.	Lattice constant, nm		CSD size, nm			
		a	c	hkl			
				(001)	(111)	(100)	(002)
473	3.7	0.3637	0.5703	21	25	32	32
523	3.4	0.3640	0.5703	13	28	28	37
573	4.4	0.3644	0.5710	26	25	33	47
623	2.2	0.3645	0.5717	16	24	33	31
673	1.0	0.3647	0.5729	20	–	39	–
723	1.9	0.3647	0.5743	26	25	33	47

The values of lattice constants for the films obtained at different substrate temperatures, calculated by the Nelson–Riley method, are shown in Table 1. It was established that the lattice parameters increase monotonically with increasing T_s from 473 to 723 K. Lattice parameter a varies from 0.3637 to 0.3647 nm, while c varies from 0.5703 to 0.5743 nm. Experimentally calculated values of (a, c) for SnS_2 are in good agreement with the values presented in the database (COD) for single crystals (i.e. a = 0.36380 nm, c = 0.58800 nm). However, the value of the lattice constant c is slightly less than the value given by the reference data, which may be due to the presence of point defects in the crystal lattice caused

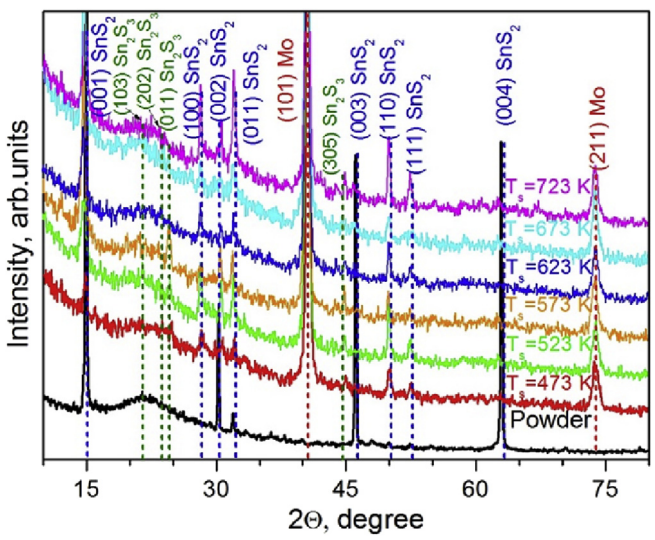

Fig. 3. XRD pattern of the powder and samples obtained at different substrate temperatures.

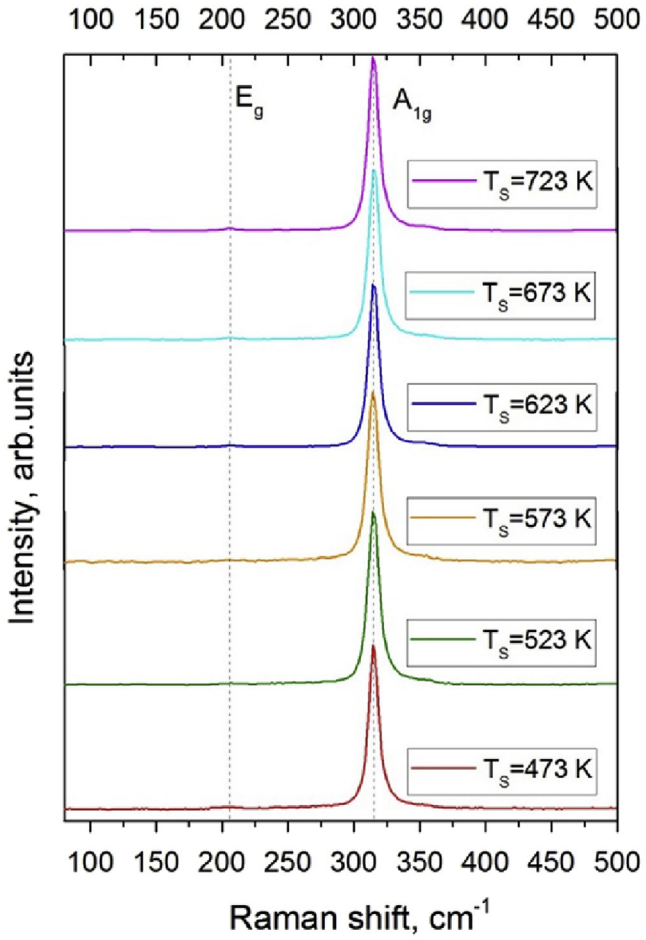

Fig. 4. Raman spectra of the SnS_2 thin films obtained at different substrate temperatures.

Please cite this article in press as: A. Voznyi, et al., Structural and electrical properties of SnS_2 thin films, Materials Chemistry and Physics (2016), http://dx.doi.org/10.1016/j.matchemphys.2016.01.036

by the deviation from stoichiometry. Similar values of lattice constant were obtained in [15] for SnS_2 films deposited by the plasma-chemical vacuum deposition method.

The results of the determination of the CSD size in the films are presented in Table 1. The calculations were performed for the directions perpendicular to the (001), (100), (002), and (100) crystallographic planes. Analysis of the obtained results shows that substrate temperature affects the CSD size in a complicated way. Namely, no trend between the substrate temperature and CSD sizes calculated for the directions perpendicular to the (001) and (002) crystallographic planes was observed. Moreover, the CSD size in the directions perpendicular to the (111) and (100) crystallographic planes was only slightly dependent on Ts. Similar values of the CSD size of 25.8 nm [by broadening the (111) line] were obtained for films obtained at the substrate temperature of 523 K. It could be concluded that there is no clear relationship between substrate temperature and the crystal quality of the samples, probably due to the combined effect of the random orientation of the crystallites and lattice defects in XRD patterns.

Fig. 4 shows the Raman scattering spectra for the samples.

It can be seen from Fig. 4 that the spectra of the samples obtained at different values of T_s are almost identical. Raman analysis of the SnS_2 thin films confirmed the presence of SnS_2 with a peak at 314.5 cm^{-1} and a weak peak at 205.6 cm^{-1}. According to theoretical [31] and experimental works [31,32,62], these peaks of SnS_2 are related to the A_{1g} and E_g modes, respectively. The FWHM of the peak dominating the A_{1g} mode was no more than 12 cm^{-1}, which indicates a high structural quality of the films. As only the A_{1g} and E_g modes were detected, we can conclude that the obtained films have 2H structure of the SnS_2 polytype [62,63]. Thus, these results confirm the data of the XRD study indicating that films have a single-phase hexagonal structure. In spite of the fact that traces of the Sn_2S_3 phase were observed on XRD patterns, the Sn_2S_3-related modes were not detected by Raman spectroscopy. This can be explained by the fact that green laser excitation radiation ($\lambda = 514$ nm) was mostly adsorbed at the surface of SnS_2, while Sn_2S_3 phase probably formed near the substrate.

Fig. 5 shows the dark current voltage characteristics in a double logarithmic plot as well as the results of their differentiation $\eta = d(\lg I)/d(\lg V)$ and $\sigma(T)$ dependencies of Sn/SnS_2/Mo sandwich structures for SnS_2 samples obtained at different substrate temperatures.

The values of conductivity of the SnS_2 films determined in the ohmic region (low-voltage region) of the I–V curves are shown in Table 2. As can be seen from Table 2, in general, conductivity increases from 3.44×10^{-7} to 1.80×10^{-4} $Om^{-1} \cdot cm^{-1}$ with substrate temperature. The only sample obtained at 673 K shows a lower conductivity of 1.79×10^{-7} $Om^{-1} \cdot cm^{-1}$ than the sample obtained at 623 K. The high resistance of the sample may be related to the high compensation of the material.

It should be noted that the obtained results of the conductivity of the SnS_2 samples are in good agreement with literature data. For example, in other works [22,64] where SnS_2 films were deposited by thermal vacuum evaporation, the conductivity of the samples

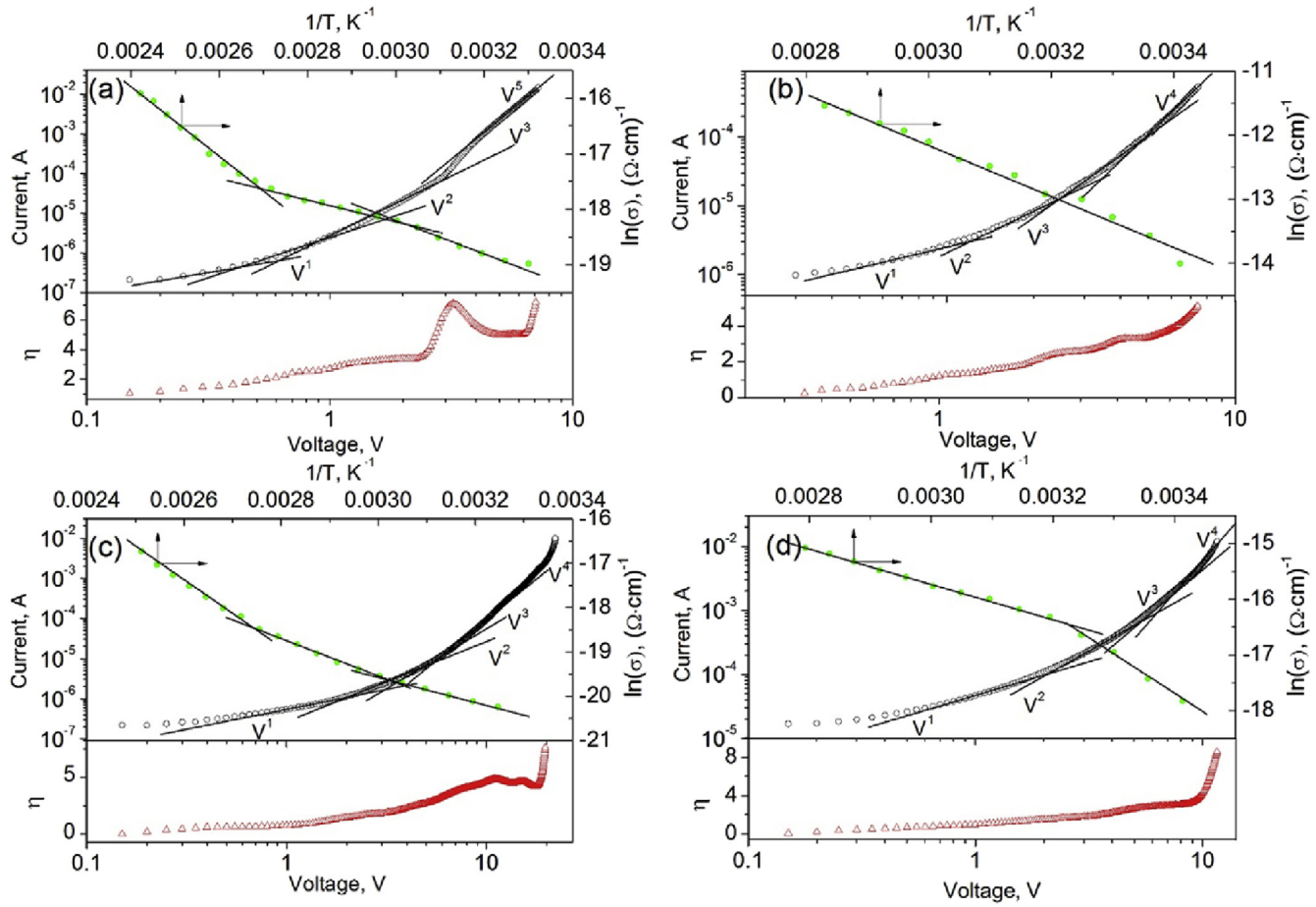

Fig. 5. I–V curves (open circles) of Sn/SnS_2/Mo sandwich structures measured at room temperature, the results of their differentiation η (open triangles) and log $\sigma(1/T)$ dependencies (filled circles) of the SnS_2 thin films obtained at substrate temperatures of 473 K (a), 573 K (b), 623 K (c), and 673 K (d).

Please cite this article in press as: A. Voznyi, et al., Structural and electrical properties of SnS_2 thin films, Materials Chemistry and Physics (2016), http://dx.doi.org/10.1016/j.matchemphys.2016.01.036

Table 2
Parameters of localized centres in SnS_2 films obtained from analysis of SCLC I–V and σ(T) functions.

T_s, K	Conductivity σ, $(Om \cdot cm)^{-1}$	From SCLC				From σ(T) dependencies	
		Manfredotti [42]		Nespurek [40]			
		E_t, eV	N_t, cm^{-3}	E_t, eV	N_t, cm^{-3}	Activation energy E_a, eV	
						This paper	Reference
473	3.44×10^{-7}					0.16	0.14 [41,64]
							0.15 [41,65]
							0.18 [40]
						0.26	0.25 [14,39]
							0.26 [22]
		0.372	2.99×10^{14}	0.372	5.09×10^{14}		
		0.389	2.52×10^{14}	0.392	2.18×10^{14}		0.40 [17,40,66]
		0.479	1.88×10^{14}	0483	3.31×10^{14}		
		0.542	1.31×10^{14}	0.545	1.66×10^{14}	0.55	
523	8.05×10^{-7}					0.35	
		0.468	3.98×10^{14}	0.477	3.63×10^{14}		
		0.495	3.47×10^{14}	0.498	4.09×10^{14}		
		0.522	5.64×10^{14}	0.522	6.66×10^{14}		0.52 [40]
573	1.60×10^{-5}					0.30	
		0.383	4.28×10^{14}	0.392	4.35×10^{14}		
		0.417	4.13×10^{14}	0.420	6.14×10^{14}	0.43	0.40 [17,40,66]
623	1.56×10^{-5}					0.25	0.25 [14,39]
							0.26 [22]
						0.37	0.37 [16]
		0.438	1.03×10^{15}	0.444	3.07×10^{15}		
		0.465	7.47×10^{14}	0.465	7.47×10^{14}		
		0.499	5.08×10^{14}	0.499	5.12×10^{14}		
		0.539	5.43×10^{14}	0.545	6.18×10^{14}		
		0.555	6.94×10^{14}	0.559	7.77×10^{14}		
						0.62	0.61 [40]
673	1.79×10^{-7}					0.26	0.25 [14,39]
							0.26 [22]
		0.383	4.28×10^{14}	0.398	1.29×10^{15}		0.37 [16]
		0.417	4.13×10^{14}	0.416	4.46×10^{14}		0.40 [17,40,66]
						0.62	0.61 [40]
723	1.80×10^{-4}					0.26	0.25 [14,39]
							0.26 [22]
		0.349	3.13×10^{14}	0.352	3.52×10^{14}		
		0.371	2.61×10^{14}	0.372	3.45×10^{14}	0.40	0.40 [17,40,66]

ranged from 10^{-4} to 6×10^{-5} $Om^{-1} \cdot cm^{-1}$. Also, values of conductivity similar to ours were obtained in the works [14,16]. However, the conductivity of the samples is lower than the value of 1.37×10^{-1} $Om^{-1} \cdot cm^{-1}$observed in [17].

There are two or three linear sections with various slopes that are observed on the Arrhenius plot of conductivity (Fig. 5). The angles of the slope generally decrease with the temperature of measurement. This behaviour is typical for the material that contains several types of donors with different activation energy [67].

However, for samples obtained at $T_s = 473$ and 673 K, the linear sections wherein the slope to the reciprocal temperature axis increases with decreasing temperature of measurement. This phenomenon can be explained by the presence of acceptor centres along with the donor centres in SnS_2 films. Such a structure of charged defects is typical for compensated materials [68] whose properties are close to those of intrinsic semiconductors. The influence of compensation begins to manifest itself at lower temperatures when the concentration of electrons becomes close to the concentration of acceptor impurities. The slope of the Arrhenius plot of conductivity increases from the value of $E_a/2k$ up to the value of E_a/k, making it possible to define the activation energy for electrically active centres.

The numbers of active centres with activation energies of $E_{a1} = 0.16$, $E_{a2} = (0.25–0.26)$, $E_{a3} = 0.30$, $E_{a4} = 0.35–0.37$, $E_{a5} = (0.40–0.43)$, $E_{a6} = 0.55$, and $E_{a7} = 0.62$ eV were determined. The accuracy of the calculations does not exceed the value of kT ~0.02 eV. The summarized results of the obtained activation energies are shown in Table 2. As follows from Table 2, in SnS_2 films deposited at substrate temperatures of 473, 623, 673, and 723 K, the activation energies of donor centres are 0.25 and 0.26 eV. The same energies of the trap levels are observed in SnS_2 films obtained by vacuum thermal evaporation [22] and spray pyrolysis methods [14].

In contrast to our results, in [39] wo activation energies were found: 0.20 eV in the temperature range of 300–365 K and 0.47 eV in the range of 365–400 K. In the paper [22], the two-step activation process was also observed. The activation energy of the donors was 0.26 eV below 242 K and 0.47 eV above 242 K.

Typical I–V curves of the sandwich structures based on SnS_2 films are shown in Fig. 5. Their shape was typical for SCLC mode. Additionally, the SCLC mode of current flow was confirmed using the procedure described in [69]. In the I–V characteristics in the high voltage range, several linear sections with different slopes to the V-axis, corresponding to $I–V^1$, $I–V^2$, $I–V^3$ and $I–V^4$ dependencies, were found. These features of I–V curves are distinguished well in the η(logV) dependencies. Each point of this graph corresponds to the slope of the current–voltage curve to the V-axis in double logarithmic scale. As was mentioned before, η(logV) dependencies were obtained by the first derivative of each experimental point of the I–V curve in the mode of SCLC.

As shown elsewhere [52,55], the IS method allows one to obtain $h(E) = 1/e \cdot d\rho/dE_F – E_F$ dependencies directly from the I–V

Please cite this article in press as: A. Voznyi, et al., Structural and electrical properties of SnS_2 thin films, Materials Chemistry and Physics (2016), http://dx.doi.org/10.1016/j.matchemphys.2016.01.036

dependencies. This method makes it possible to reconstruct the energy distribution of traps in the band gap of the material. The depth and concentration of the parameters of LSs were determined by the position of the maxima in the h(E) dependencies. For the processing of the experimental data we used the low-temperature approximation method of IS [52]. Simplified equations of the method that contained only the first [56] and both the first and second derivatives [54] were used. Some results of the reconstruction of the energy distribution of the energy traps in the samples using the simplifications proposed by Manfredotti [42] and Nespurek [54] are shown in Fig. 6 (a–c).

The results of calculations of the parameters of LSs in the SnS_2 films obtained at different substrate temperatures are shown in Table 2. Using this method, a number of traps were identified with energies of $E_{t1} = (0.52–0.55)$, $E_{t2} = (0.46–0.49)$, $E_{t3} = (0.43–0.45)$, and $E_{t4} = (0.35–0.39)$. The accuracy of the calculations does not exceed kT. The concentration of these LSs is in the range of 2×10^{14} to 3×10^{15} cm^{-3}.

The results were checked by reconstruction of the I–V curve with the use of the defined values of E_t and N_t. The procedure of I–V curve reconstruction is described in [52]. An example of the reconstructed I–V curve is shown in Fig. 6(d). As can be seen from this figure, the reconstructed curve is in good agreement with experimental data at a low voltage range, which confirms the results of our calculations. The difference between these curves at high voltages is associated with the possible presence of shallower LSs in the samples. These energy levels cannot be detected by the IS method and hence they were not considered in the reconstruction of I–V curves.

As mentioned above, it is difficult to identify the activation energies of the obtained traps and donor centres since there are no theoretical works related to the calculation of the formation and ionization energies of point defects in SnS_2. We speculate that, analogously to S-rich SnS [42,43] shallow states with activation energies of about 0.26 and 0.4 eV could be assigned to single- and double-charged interstitial Sn, while the deep centre of about 0.6 eV is related to the vacancy of sulfur.

4. Conclusions

In this paper, a comprehensive study of the structural and electrical properties of SnS_2 thin films was performed.

It was established that the tin disulfide films consist of platelet-shaped grains. The average grain size varies in the range of 0.7–1.2 μm and depends on the substrate temperature. All layers were close to stoichiometric composition. Namely, the atomic concentrations of the compound components are 35 and 65% for Sn and S, respectively.

X-ray analysis shows that the films obtained in the temperature range of 473–723 K contained mostly the hexagonal phase of SnS_2.

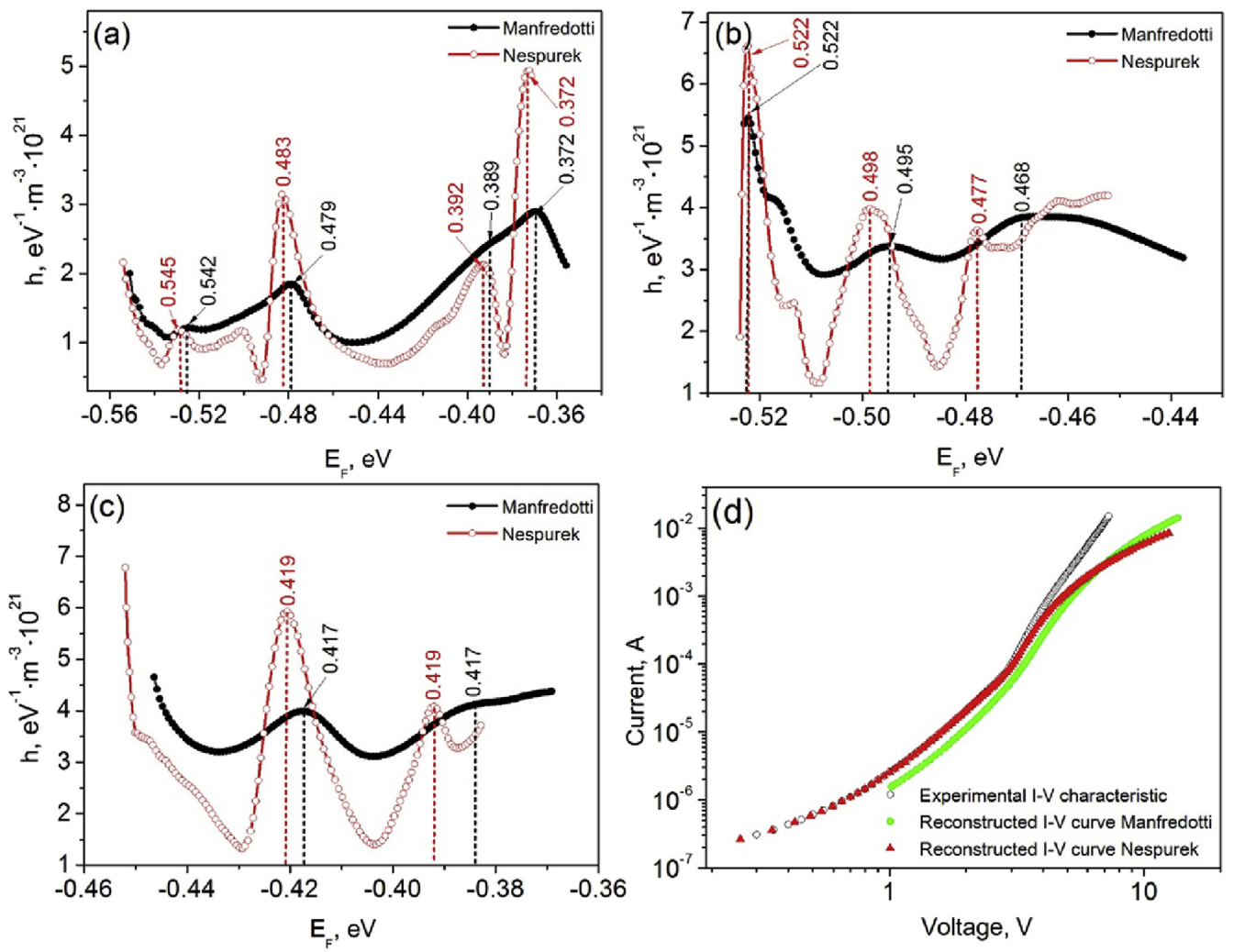

Fig. 6. The energy trap distribution in the band gap of the material for $T_s = 473$ K (a), 523 K (b), and 573 K (c) and typical experimental and simulated I–V curves for $T_s = 473$ K (d).

Please cite this article in press as: A. Voznyi, et al., Structural and electrical properties of SnS_2 thin films, Materials Chemistry and Physics (2016), http://dx.doi.org/10.1016/j.matchemphys.2016.01.036

Also, the films include small amounts (<3–5%) of Sn_2S_3 compound, most likely near the substrate. All samples have [002] texture. The lattice constants (a and c) increase monotonically from 0.3637 to 0.3647 nm and from 0.5703 to 0.5743 nm, respectively, with increasing substrate temperature from 473 to 723 K.

Analysis of the samples microstructure reveals no clear relationship between coherent scattering domain size and substrate temperature.

Raman analysis showed that the SnS_2 films are single-phase and have hexagonal structure.

The conductivity of the SnS_2 films increases in a wide range from 1.79×10^{-7} to 1.80×10^{-4} $Om^{-1} \cdot cm^{-1}$ with increases in substrate temperature from 473 to 723 K.

From the Arrhenius plot of conductivity–temperature dependencies, the activation energies of donor impurity are determined. In particular, activation energies of about 0.2, 0.3, 0.4, and 0.6 eV were found.

By analysis of the I–V dependencies in the space-charge limited current mode, the localized states in the band gap of the SnS_2 thin films with energy depths of $E_{t1} = (0.52–0.55)$, $E_{t2} = (0.46–0.49)$, $E_{t3} = (0.43–0.45)$, and $E_{t4} = (0.35–0.39)$ were established. The concentration of these localized states lies in the range of 2×10^{14} to 3×10^{15} cm^{-3}.

Acknowledgments

This work was supported by the State Fund for Fundamental Research (project no. GP/F61/087) and Ministry of Education and Science of Ukraine (Grant nos. 0113U000131 and 0112U000772) grants. A. Voznyi and Dr. V. Kosyak acknowledge the Erasmus Mundus Ianus II programme.

References

[1] M. Thripuranthaka, D.J. Late, Temperature dependent phonon shifts in single-layer WS_2, ACS Appl. Mater. Interface 6 (2014) 1158–1163, http://dx.doi.org/10.1021/am404847d.

[2] P.K. Kannan, D.J. Late, H. Morgan, C.S. Rout, Recent developments in 2D layered inorganic nanomaterials for sensing, Nanoscale 7 (2015) 13293–13312, http://dx.doi.org/10.1039/C5NR03633J.

[3] D.J. Late, P.A. Shaikh, R. Khare, R.V. Kashid, M. Chaudhary, M.A. More, et al., Pulsed laser-deposited MoS_2 thin films on W and Si: field emission and photoresponse studies, Appl. Mater. Interface 6 (2014) 15881–15888, http://dx.doi.org/10.1021/am503464h.

[4] J. George, K.S. Joseph, Absorption edge measurements in tin disulphide thin films, J. Phys. D. Appl. Phys. 15 (2000) 1109–1116, http://dx.doi.org/10.1088/0022-3727/15/6/021.

[5] H. Cohen, Z. Esterlit, R. Brener, E. Lifshitz, T. Maniv, M. Folman, Reflection electron energy loss spectroscopy study of 2H-SnS_2 single crystals, Mater. Sci. Forum 91–93 (1992) 733–738, http://dx.doi.org/10.4028/. www.scientific.net/MSF.91-93.733.

[6] J.P. Gowers, P.A. Lee, Mobility of electrons in SnS_2 single crystals, Solid State Commun. 8 (1970) 1447–1449, http://dx.doi.org/10.1016/0038-1098(70)90716-7.

[7] Y. Huang, E. Sutter, J.T. Sadowski, M. Cotlet, O.L.A. Monti, D.A. Racke, et al., Tin disulfide - an emerging layered metal dichalcogenide semiconductor: materials properties and device characteristics, ACS Nano 8 (2014) 10743–10755, http://dx.doi.org/10.1021/nn504481r C2014.

[8] L.A. Burton, D. Colombara, R.D. Abellon, F.C. Grozema, L.M. Peter, T.J. Savenije, et al., Synthesis, characterization, and electronic structure of single-crystal SnS, Sn_2S_3, and SnS_2, Chem. Mater 25 (2013) 4908–4916, http://dx.doi.org/10.1021/cm403046m.

[9] J. Camassel, M. Schlüter, S. Kohn, J.P. Voitchovsky, Y.R. Shen, M.L. Cohen, Wavelength modulation spectra and electronic band structure of SnS_2 and $SnSe_2$, Phys. Status Solidi 75 (1976) 303–314, http://dx.doi.org/10.1002/pssb.2220750133.

[10] S. Nakashima, H. Katahama, A. Mitsuishi, The effect of polytypism on the vibrational properties of SnS_2, Phys. B+C 105 (1981) 343–346, http://dx.doi.org/10.1016/0378-4363(81)90272-2.

[11] A.K. Abass, H.A. Jassim, K.J. Majeid, R.H. Misho, Optical parameters of chemically deposited tin disulphide, Phys. Status Solidi 91 (1985) 129–133, http://dx.doi.org/10.1002/pssa.2210910117.

[12] H. Zhong, G. Yang, H. Song, Q. Liao, H. Cui, P. Shen, et al., Vertically aligned graphene-like SnS_2 ultrathin nanosheet arrays: excellent energy storage, catalysis, photoconduction, and field-emitting performances, J. Phys. Chem. C 116 (2012) 9319–9326, http://dx.doi.org/10.1021/jp301024d.

[13] C. Shi, Z. Chen, G. Shi, R. Sun, X. Zhan, X. Shen, Influence of annealing on characteristics of tin disulfide thin films by vacuum thermal evaporation, Thin Solid Films 520 (2012) 4898–4901, http://dx.doi.org/10.1016/j.tsf.2012.03.050.

[14] L. Amalraj, C. Sanjeeviraja, M. Jayachandran, Spray pyrolysised tin disulphide thin film and characterisation, J. Cryst. Growth 234 (2002) 683–689, http://dx.doi.org/10.1016/S0022-0248(01)01756-0.

[15] S. Wang, S. Wang, J. Chen, P. Liu, M. Chen, H. Xiong, et al., Influence of the deposition parameters on the properties of SnS_2 films prepared by PECVD method combined with solid sources, J. Nanoparticle Res. 16 (2014) 2610, http://dx.doi.org/10.1007/s11051-014-2610-0.

[16] B.R. Sankapal, R.S. Mane, C.D. Lokhande, Successive ionic layer adsorption and reaction (SILAR) method for the deposition of large area (approximately 10 cm^2) tin disulfide (SnS_2) thin films, Mater. Res. Bull. 35 (2000) 2027–2035, http://dx.doi.org/10.1016/S0025-5408(00)00405-0.

[17] T. Shibata, Y. Muranushi, T. Miura, T. Kishi, Electrical characterization of 2H-SnS_2 single crystals synthesized by the low temperature chemical vapor transport method, J. Phys. Chem. Solids 52 (1991) 551–553, http://dx.doi.org/10.1016/0022-3697(91)90190-B.

[18] N.G. Deshpande, A.A. Sagade, Y.G. Gudage, C.D. Lokhande, R. Sharma, Growth and characterization of tin disulfide (SnS_2) thin film deposited by successive ionic layer adsorption and reaction (SILAR) technique, J. Alloys Compd. 436 (2007) 421–426, http://dx.doi.org/10.1016/j.jallcom.2006.12.108.

[19] K.S. Kumar, C. Manoharan, L. Amalraj, S. Dhanapandian, G. Kiruthigaa, K. Vijayakumar, Spray deposition and characterization of undoped and in-doped tin disulphide thin films, Cryst. Res. Technol. 47 (2012) 771–779, http://dx.doi.org/10.1002/crat.201100349.

[20] B. Thangaraju, P. Kaliannan, Spray pyrolytic deposition and characterization of SnS and SnS_2 thin films, J. Phys. D. - Appl. Phys. 33 (2000) 1054–1059, http://dx.doi.org/10.1088/0022-3727/33/9/304.

[21] C. Khélia, K. Boubaker, T. Ben Nasrallah, M. Amlouk, S. Belgacem, Morphological and thermal properties of β-SnS_2 sprayed thin films using Boubaker polynomials expansion, J. Alloys Compd. 477 (2009) 461–467, http://dx.doi.org/10.1016/j.jallcom.2008.10.051.

[22] K. Kawano, R. Nakata, M. Sumita, Effects of substrate temperature on absorption edge and photocurrent in evaporated amorphous SnS_2 films, J. Phys. D. Appl. Phys. 136 (1989) 136–141, http://dx.doi.org/10.1088/0022-3727/22/1/019.

[23] S.K. Panda, A. Antonakos, E. Liarokapis, S. Bhattacharya, S. Chaudhuri, Optical properties of nanocrystalline SnS_2 thin films, Mater. Res. Bull. 42 (2007) 576–583, http://dx.doi.org/10.1016/j.materresbull.2006.06.028.

[24] K.T.R. Reddy, M.V. Reddy, M. Leach, J.K. Tan, D.Y. Jang, R.W. Miles, Crystalline behaviour of SnS layers produced by sulfurization of Sn films using H_2S, AIP Conf. Proc. 1447 (2012) 709–710, http://dx.doi.org/10.1063/1.4710200.

[25] C. Shi, P. Yang, M. Yao, X. Dai, Z. Chen, Preparation of SnS_2 thin films by close-spaced sublimation at different source temperatures, Thin Solid Films 534 (2013) 28–31, http://dx.doi.org/10.1016/j.tsf.2013.01.072.

[26] A.S. Opanasyuk, D.I. Kurbatov, V.V. Kosyak, S.I. Kshniakina, S.N. Danilchenko, Characteristics of structure formation in zinc and cadmium chalcogenide films deposited on nonorienting substrates, Crystallogr. Rep. 57 (2012) 927–933, http://dx.doi.org/10.1134/S1063774512070206.

[27] Y.P. Gnatenko, P.M. Bukivskij, S. Opanasyuk, D.I. Kurbatov, M.M. Kolesnyk, V.V. Kosyak, et al., Low-temperature photoluminescence of II-VI films obtained by close-spaced vacuum sublimation, J. Lumin 132 (2012) 2885–2888, http://dx.doi.org/10.1016/j.jlumin.2012.06.003.

[28] V. Kosyak, A. Opanasyuk, P.M. Bukivskij, Y.P. Gnatenko, Study of the structural and photoluminescence properties of CdTe polycrystalline films deposited by close-spaced vacuum sublimation, J. Cryst. Growth 312 (2010) 1726–1730, http://dx.doi.org/10.1016/j.jcrysgro.2010.02.034.

[29] M.G. Sousa, A.F. da Cunha, P.A. Fernandes, Annealing of RF-magnetron sputtered SnS_2 precursors as a new route for single phase SnS thin films, J. Alloys Compd. 592 (2014) 80–85, http://dx.doi.org/10.1016/j.jallcom.2013.12.200.

[30] C. Manoharan, K. Santhosh Kumar, S. Dhanapandian, G. Kiruthigaa, Preparation and physical investigations on sprayed Sn_xS_y thin films for solar cell applications, Nanosci. Eng. Technol. 11 (2011) 263–268, http://dx.doi.org/10.1109/ICONSET.2011.61934.

[31] V.G. Hadjiev, D. De, H.B. Peng, J. Manongdo, A.M. Guloy, Phonon probe of local strains in SnS_xSe_{2-x} mixed crystals, Phys. Rev. B 87 (2013) 104302, http://dx.doi.org/10.1103/PhysRevB.87.104302.

[32] H.R. Chandrasekhar, R.G. Humphreys, U. Zwick, M. Cardona, Infrared and Raman spectra of the IV-VI compounds SnS and SnSe, Phys. Rev. B 15 (1977) 2177–2183, http://dx.doi.org/10.1103/PhysRevB.15.2177.

[33] J. Malaquias, P.A. Fernandes, P.M.P. Salomé, A.F. da Cunha, Assessment of the potential of tin sulphide thin films prepared by sulphurization of metallic precursors as cell absorbers, Thin Solid Films 519 (2011) 7416–7420, http://dx.doi.org/10.1016/j.tsf.2011.01.393.

[34] E. Lifshitz, Z. Chen, L. Bykov, Optical spectroscopy of 1T-SnS_2 single crystal, J. Phys. Chem. 97 (1993) 238–242, http://dx.doi.org/10.1021/nl1017173.

[35] L. Sharp, D. Soltz, B.A. Parkinson, Growth and characterization of tin disulfide single crystals, Cryst. Growth Des. 6 (2006) 1523–1527, http://dx.doi.org/10.1021/cg050335y.

[36] T. Shibata, N. Kambe, Y. Muranushi, T. Miura, T. Kishi, Optical characterisation of single crystal 2H-SnS_2 synthesised by the chemical vapour transport

Please cite this article in press as: A. Voznyi, et al., Structural and electrical properties of SnS_2 thin films, Materials Chemistry and Physics (2016), http://dx.doi.org/10.1016/j.matchemphys.2016.01.036

method at low temperatures, J. Phys. D. Appl. Phys. 23 (1990) 719–723, http://dx.doi.org/10.1088/0022-3727/23/6/014.
[37] S. Mandalidis, J.A. Kalomiros, K. Kambas, A.N. Anagnostopoulos, Optical investigation of SnS_2 single crystals, J. Mater. Sci. 31 (1996) 5975–5978, http://dx.doi.org/10.1007/BF01152147.
[38] T. Shibata, T. Miura, T. Kishi, T. Nagai, Synthesis of single crystal SnS_2 by chemical vapor transport method at low temperature using reverse temperature gradient, J. Cryst. Growth 106 (1990) 593–604, http://dx.doi.org/10.1016/0022-0248(90)90032-G.
[39] J. George, K.S. Joseph, Effect of heating on the electrical and optical properties of tin disulphide thin films, J. Phys. D. Appl. Phys. 16 (1982) 33–38, http://dx.doi.org/10.1088/0022-3727/16/1/007.
[40] S.G. Patil, R.H. Tredgold, Electrical and photoconductive properties of SnS_2 crystals, J. Phys. D. Appl. Phys. 4 (1971) 718–722, http://dx.doi.org/10.1088/0022-3727/4/5/312.
[41] A. Sanchez-Juarez, A. Ortiz, Effects of precursor concentration on the optical and electrical properties of Sn_xS_y thin films prepared by plasma-enhanced chemical vapour deposition, Semicond. Sci. Technol. 17 (2002) 931–937, http://dx.doi.org/10.1088/0268-1242/17/9/305.
[42] J. Vidal, S. Lany, M. d'Avezac, A. Zunger, A. Zakutayev, J. Francis, et al., Band-structure, optical properties, and defect physics of the photovoltaic semiconductor SnS, Appl. Phys. Lett. 100 (2012) 032104, http://dx.doi.org/10.1063/1.3675880.
[43] B.D. Malone, A. Gali, E. Kaxiras, First principles study of point defects in SnS, Phys. Chem. Chem. Phys. 16 (2014) 26176–26183, http://dx.doi.org/10.1039/C4CP03010A.
[44] A.D. Pogrebnjak, T.O. Berestok, A.S. Opanasyuk, Y. Takeda, K. Oyoshi, F.F. Komarov, et al., Structural properties and elemental composition of Au^+ implanted ZnO films, obtained by sol-gel method, J. NANO- Electron. Phys. 6 (2014) 1–5.
[45] R.H. Williams, R.B. Murray, D.W. Govan, J.M. Thomas, E.L. Evans, Band structure and photoemission studies of SnS_2 and $SnSe_2$. I. Experimental, J. Phys. C Solid State Phys. 6 (1973) 3631–3642, http://dx.doi.org/10.1088/0022-3719/6/24/022.
[46] R.K. Willardson, A.C. Beer, Semiconductors and Semimetals: Contacts, Junctions, Emitters, Academic Press, 1981 (Accessed December 2, 2015), https://books.google.com/books?id=SNk9FfcwQSUC&pgis=1.
[47] S. Kodigala, Thin Film Solar Cells from Earth Abundant Materials, Elsevier, 2013 (Accessed December 2, 2015), https://www.elsevier.com/books/thin-film-solar-cells-from-earth-abundant-materials/kodigala/978-0-12-394429-0.
[48] R. Scheer, H.-W. Schock, Chalcogenide Photovoltaics: Physics, Technologies, and Thin Film Devices, Wiley, 2011 (Accessed December 2, 2015), http://onlinelibrary.wiley.com/book/10.1002/9783527633708.
[49] D. Kurbatov, V. Kosyak, A. Opanasyuk, V. Melnik, Native point defects in ZnS films, Phys. B Condens. Matter 404 (2009) 5002–5005, http://dx.doi.org/10.1016/j.physb.2009.08.197.
[50] V.V. Kosyak, M.M. Kolesnyk, A.S. Opanasyuk, Point defect structure in CdTe and ZnTe thin films, J. Mater. Sci. Mater. Electron 19 (2008) 375–381, http://dx.doi.org/10.1007/s10854-007-9562-4.
[51] J.C. Pfister, Note on the interpretation of space charge limited currents with traps, Phys. Status Solidi 24 (1974) K15–K17, http://dx.doi.org/10.1002/pssa.2210240140.
[52] A.S. Opanasyuk, N.N. Opanasyuk, N.V. Tirkusova, High-temperature injection spectroscopy of deep traps in CdTe polycrystalline films, Semicond. Phys. Quantum Electron. Optoelectron 6 (2003) 444–449.
[53] F. Stockmann, An exact evaluation of steady-state space-charge-limited currents for arbitrary trap distributions, Phys. Stat. Sol. A 64 (1981) 475–483, http://dx.doi.org/10.1002/pssa.2210640209.
[54] O. Zmeskal, F. Schauer, S. Nespurek, The bulk trap spectroscopy of solids by temperature- modulated space-charge-limited currents, J. Phys. C Solid State Phys. 18 (1985) 1873–1884.
[55] D. Kurbatov, A. Opanasyuk, H. Khlyap, Injection and optical spectroscopy of localized states in II-VI semiconductor films, Adv. Asp. Spectrosc. (2012) 499–538, http://dx.doi.org/10.5772/48290.
[56] A.M. Mancini, C. Manfredotti, C. De Blasi, G. Micocci, A. Tepore, Characterization of CdTe with photoelectronic techniques, Rev. Phys. Appliquée 12 (1977) 255–261, http://dx.doi.org/10.1051/rphysap:01977001202025500.
[57] O. Madelung, Semiconductors: Data Handbook, Springer Berlin Heidelberg, Berlin, Heidelberg, 2004, http://dx.doi.org/10.1007/978-3-642-18865-7.
[58] A.A. Voznyi, V.V. Kosyak, A.S. Opanasyuk, V.M. Kuznetsov, Structural properties of the Sn_xS_y films obtained by the Thermal vacuum co-evaporation, Proc. Int. Conf. Nanomater. Appl. Prop. (2014) 1–4.
[59] S. Prasert, Development of Earth-abundant Tin (II) Sulfide Thin-film Solar Cells by Vapor Deposition, 2013. http://nrs.harvard.edu/urn-3:HUL.InstRepos:11051177.
[60] L.S. Price, I.P. Parkin, A.M.E. Hardy, R.J.H. Clark, T.G. Hibbert, K.C. Molloy, Atmospheric pressure chemical vapor deposition of tin sulfides (SnS, Sn_2S_3, and SnS_2) on glass, Chem. Mater 11 (1999) 1792–1799, http://dx.doi.org/10.1021/cm990005z.
[61] K. Vijayakumar, C. Sanjeeviraja, M. Jayachandran, L. Amalraj, Characterization of Tin disulphide thin films prepared at different substrate temperature using spray pyrolysis technique, J. Mater. Sci. Mater. Electron 22 (2011) 929–935, http://dx.doi.org/10.1007/s10854-010-0239-z.
[62] H. Katahama, Raman scattering study of interlayer bonding in CdI_2 and SnS_2 under hydrostatic pressure: analysis by use of Van Der Waals interaction, J. Phys. Chem. Solids 44 (1983) 1081–1087, http://dx.doi.org/10.1016/0022-3697(83)90091-4.
[63] A.J. Smith, P.E. Meek, W.Y. Liang, Raman scattering studies of SnS_2 and $SnSe_2$, J. Phys. C Solid State Phys. 10 (1977) 1321–1323, http://dx.doi.org/10.1088/0022-3719/10/8/035.
[64] D. O'Hare, W. Jaegermann, D.L. Williamson, F.S. Ohuchi, B.A. Parkinsont, X-ray photoelectron, Moessbauer, magnetic and electrical conductivity study of $SnS_2\{CoCp_2\}_{0.31}$, Inorg. Chem. 27 (1988) 1537–1542, http://dx.doi.org/10.1021/ic00282a006.
[65] W. Jaegerrnann, F.S. Ohuchi, B.A. Parkinson, Electrochemical and solid state reactions of copper with n-SnS_2, Ber. Bunsenges. Phys. Chem. 93 (1989) 29–37, http://dx.doi.org/10.1002/bbpc.19890930107.
[66] J. George, C.K.V. Kumari, Electrical characterization of tin disulphide crystals, Solid State Commun. 49 (1984) 103–106, http://dx.doi.org/10.1016/0038-1098(84)90572-6.
[67] M. Grundmann, The Physics of Semiconductors, Springer Berlin Heidelberg, Berlin, Heidelberg, 2010, http://dx.doi.org/10.1007/978-3-642-13884-3.
[68] G.S. Gildenblat, A.R. Rao, Current-voltage characteristic of pulsed space-charge-limited currents in GaAs, J. Appl. Phys. 61 (1987) 2683–2685, http://dx.doi.org/10.1063/1.337904.
[69] N.V. Tirkusova, A.S. Opanasyuk, I. Yu Protsenko, Some peculiarities of the reconstruction of deep traps distributions via the injecting spectroscopy method, J. Phys. Stud. 2 (2000) 208–215.

Please cite this article in press as: A. Voznyi, et al., Structural and electrical properties of SnS_2 thin films, Materials Chemistry and Physics (2016), http://dx.doi.org/10.1016/j.matchemphys.2016.01.036